Realtime Paper Shape Estimation for Origami Robot System

Hiroto ARASAKI[1], Sena TAKAHASHI[1], and Akio NAMIKI[1]

***Abstract*— In this paper, we propose a digital-twin origami simulator that can be executed simultaneously with the robot's folding operation in realtime and can represent paper folds and a realtime paper shape estimation system. The proposed origami simulator considers elasto-plastic deformation and represents the folded state of paper well. The actual origami shape is acquired from multiple depth sensors in real time as point cloud information. It is reflected in the paper shape in the origami simulator in realtime using a point cloud matching method. In experiments, paper shape estimation was performed on an actual origami paper, and accurate shape estimation was achieved.**

I. Introduction

Manipulation of flexible objects like sheets of paper is a difficult problem for robots [1]. On the other hand, a skilled person can manipulate paper at will, and Origami, a traditional Japanese art, is an example of such superior paper manipulation. Achieving such extreme dexterity is one of the goals of robotic technology.

There have been many previous studies on the manipulation of cloth or rope. However, there are few studies on paper folding. Whereas cloth has no bending elasticity, paper does, and its properties change as it is folded repeatedly. For this reason, origami robots require different manipulation strategies than those used for folding cloth. In particular, it is necessary to measure the shape and position of the paper in realtime because the paper changes its shape and position during folding.

Our research group has been studying paper manipulation by a dual multi-fingered hand robot system. So far, we have succeeded in performing valley triangular folds [2], [5], [3]. The realized folds are shown in Fig.2. However, in this experiment, the shape of the paper was not accurately estimated, and only the positions of the paper vertices were measured.

For paper shape recognition, we have also achieved shape estimation based on depth sensors and a physical paper model [4]. However, more complex folding operations have yet to be realized because the paper model does not sufficiently accommodate paper folding. Therefore, in this study, we have developed an digital-twin origami simulator that can be executed simultaneously with the robot's folding operation in realtime and can represent paper folds and a realtime paper shape estimation system.

[1]Hiroto ARASAKI, Sena TAKAHASHI, and Akio NAMIKI are with Graduate School of Engineering, Chiba University, Japan namiki@faculty.chiba-u.jp

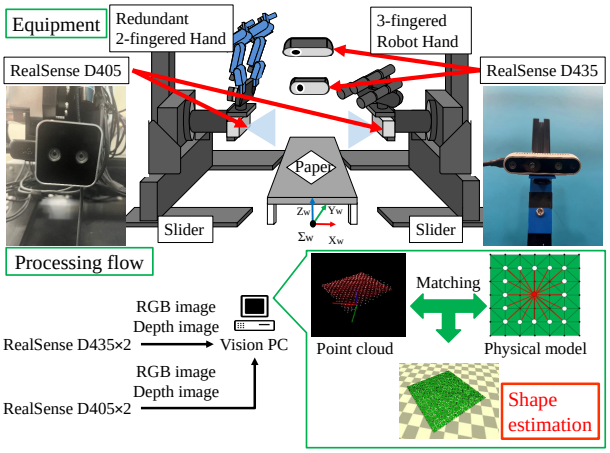

Fig. 1: Origami Robot System

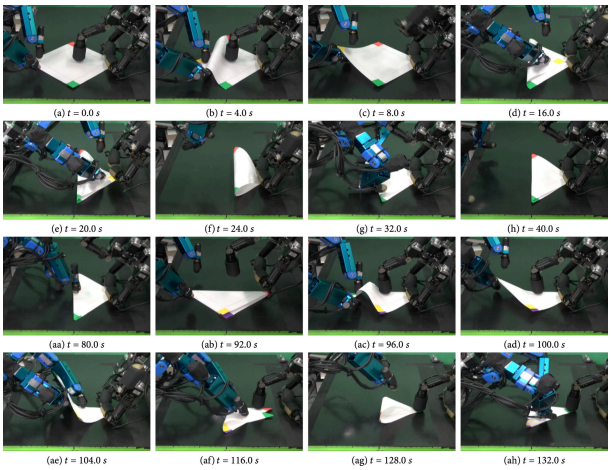

Fig. 2: Example of valley folds [5]

II. System Configuration

We developed a human-like, dual-armed, multifingered hand system for complex folding motions. The system configuration is shown in Fig.1. Each arm is a 6-DOF manipulator consisting of a linear slider with orthogonal axes and a wrist with three rotational DOF joints. A different type of multifingered hand is attached to the top of each arm. The left two-fingered hand is used for fine manipulation, and the right three-fingered hand is mainly used to hold the paper.

The left hand is a two-fingered robot hand with 7 DOFs in each finger. The number of DOFs in each finger is more than human fingers or fingers of a typical robot hand, which helps realize an extensive range of motion. The right hand

is a three-fingered robot hand with 3-DOFs on each finger.

Realsense D435 cameras are installed on the top and back side of the platform, and Realsense D405 cameras are on both wrists of the robot hand. The RGB-D image information obtained from the cameras is sent to Vision PC, which estimates the paper condition by image processing, physical simulation, and point cloud matching using Coherent Point Drift (CPD) [6], [7].

Fig.3 shows the flow of paper shape estimation. First, the shape estimation module receives RGB images from the RGB-D cameras and extracts origami regions by masking specific colors. Then, by masking the depth image from the RGB-D cameras with the extracted origami area, the 3D point cloud data of the origami is obtained. However, the point cloud data alone does not directly provide the positions of specific origami parts, such as edges and corners. If the origami is occluded from the cameras, the point cloud data is partially missing, resulting in shape estimation failure. To solve this problem, the physical simulator is run in parallel, and CPD is used to match point clouds consisting of nodes of the paper model on the physical simulator with point clouds acquired from the cameras to interpolate information about the shape. The matched point cloud can be used to obtain the position of a specific part of the paper.

III. Origami Simulator Considering Elasto-Plastic Deformation

The proposed digital-twin origami simulator that takes elasto-plastic deformation into account is explained. The origami model is shown in Fig. 4. For simplicity, springs are placed only in the red lines, and dampers for damping are not included.

A. Process in simulation

We employed Substep Extended Position Based Dynamics (Substep XPBD)[8] to achieve realtime simulation.

The origami simulator iteratively performs a prediction step and an update step. In the prediction step, the current position of each node $\boldsymbol{X}_{\text{old}}$, velocity $\boldsymbol{V}$, and external force $\boldsymbol{F}$ are used to obtain a tentative solution $\tilde{\boldsymbol{X}}$ for the position after Δt_s.

$$\tilde{\boldsymbol{X}} = \boldsymbol{X}_{\text{old}} + \Delta t_s \boldsymbol{V} + {\Delta t_s}^2 \boldsymbol{M}^{-1} \boldsymbol{F}, \tag{1}$$

where $\Delta t_s = \Delta t / N_s$ and N_s is the number of iterations of the update formula in one step.

In the update step, the position of each node is updated by spring constraints between the masses. The spring constraint keeps the distance between the two masses $\boldsymbol{x}_1$ and $\boldsymbol{x}_2$ at the natural length of the current spring, and the update formula is given as follows.

$$\boldsymbol{x}_{1i+1} = \boldsymbol{x}_{1i} + \frac{|\Delta \boldsymbol{p}| - (l + \Delta l_p)}{m_1({m_1}^{-1} + {m_2}^{-1} + \frac{\alpha_{\text{spring}}}{{\Delta t_s}^2})} \frac{\Delta \boldsymbol{p}}{|\Delta \boldsymbol{p}|}, \tag{2}$$

$$\boldsymbol{x}_{2i+1} = \boldsymbol{x}_{2i} - \frac{|\Delta \boldsymbol{p}| - (l + \Delta l_p)}{m_2({m_1}^{-1} + {m_2}^{-1} + \frac{\alpha_{\text{spring}}}{{\Delta t_s}^2})} \frac{\Delta \boldsymbol{p}}{|\Delta \boldsymbol{p}|}, \tag{3}$$

where l is the initial value of the natural length of the spring and the permanent elongation Δl_p means the amount of plastic deformation of the spring. Also, $\Delta \boldsymbol{p} = \boldsymbol{x}_{2i} - \boldsymbol{x}_{1i}$, and α_{spring} is the elastic compliance of the spring and corresponds to the reciprocal of the spring constant.

B. Integration with shape estimation results

Based on the point cloud estimated by the shape estimation module, the position of each node of the physical model is changed. We assume a virtual spring with a natural length of 0 between each node of the estimated point cloud $\boldsymbol{x}_d$ and the corresponding node of the physical simulator $\boldsymbol{x}$, and the spring moves the node of the simulator.

$$\boldsymbol{x}_{i+1} = \boldsymbol{x}_i - \frac{\boldsymbol{x}_i - \boldsymbol{x}_d}{m(m^{-1} + \frac{\alpha_{\text{input}}}{{\Delta t_s}^2})} \tag{4}$$

where α_{input} is the elastic compliance of the virtual spring for the input.

C. Elasto-plastic spring mass model

The elastoplastic spring-mass model uses bilinear plasticity and the kinematic hardening law as the spring's plasticity model. The model shows the stress-strain diagram of the Fig. 5, in which plastic deformation is proportional to the amount of deformation that occurs when the deformation exceeds the limit of elasticity.

The following is a rule for updating the model.

1) The initial permanent elongation Δl_p is 0.
2) The elastic region of elongation is set to $[\Delta l_p/a - \Delta l_Y, \Delta l_p/a + \Delta l_Y]$.
3) When the elongation Δl changes beyond the limit of elasticity by Δl_{over}, $a\Delta l_{\text{over}}$ is added to the permanent elongation Δl_p.

Δl_Y is the amount of elongation at the initial yield point and is expressed by $\Delta l_Y = \frac{\epsilon_Y}{l}$ using the yield strain ϵ_Y and the natural length of the spring l. The plasticity rate a is the ratio of plastic strain to total strain during plastic deformation.

IV. Experiment

Paper shape estimation was performed using actual origami paper. In the experiment, human hands perform "first valley fold" and "second valley fold" on a work table, followed by the opening of the folds.

The results of the experiment are shown in Fig. 6. The left side of the figure shows the estimation results and the right side shows the actual paper shape. The images are, from top to bottom, (a) first valley fold, (b) second valley fold, (c) opening the second valley fold, and (d) opening the first valley fold. It can be seen that the model follows the actual paper throughout the entire process.

V. Conclusion

In this study, we developed a paper shape estimation system with an origami simulator that can be executed simultaneously with the robot's folding operation in realtime and a realtime paper shape estimation system. The proposed origami simulator considers elasto-plastic deformation and

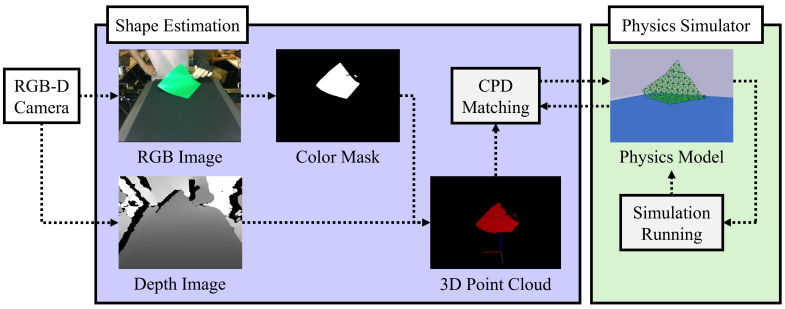

Fig. 3: Processing Flow

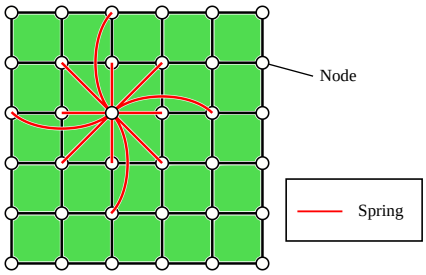

Fig. 4: Origami Simulator

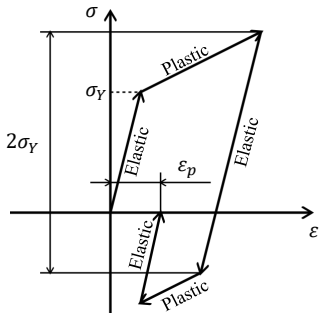

Fig. 5: Elastoplastic Model

represents the folded state of paper well. In experiments, paper shape estimation was performed on an actual origami paper, and accurate shape estimation was achieved. In the future, the proposed origami estimation system will be integrated into the robot origami operation.

REFERENCES

[1] J. Sanchez, J. A. Corrales, B. C. Bouzgarrou, and Y. Mezouar, "Robotic manipulation and sensing of deformable objects in domestic and industrial applications: a survey," International Journal of Robotics Research, vol. 37, no. 7, pp. 688?716, 2018.

[2] A. Namiki, S. Yokosawa, "Robotic origami folding with dynamic motion primitives", 2015 IEEE/RSJ Int. Conf. Intelligent Robots and Systems (IROS). IEEE. 2015, pp. 5623?5628.

[3] Robotic Origami, `https://youtu.be/hWsApBoRtfY`.

[4] R. Minowa and A. Namiki, "Origami Operations by Multifingered Robot Hand with Realtime 3D Shape Estimation of Paper" 2016 IEEE/SICE Int. Symp. System Integration, pp.729-734.

[5] A. Namiki and S. Yokosawa, "Origami Folding by Multi-Fingered Hands with Motion Primitives", Cyborg and Bionic Systems, Vol.2021, Article ID 9851834.

[6] Andriy Myronenko, Xubo Song: "Point set registration: Coherent point drift". IEEE transactions on pattern analysis and machine intelligence 32.12, pp. 2262-2275, (2010).

[7] K. Nakamura, N. Trada, and A. Akio, "Shape Matching between Paper and Physical Model with RGB-D Sensor", Proceedings, JSME Conference on Robotics and Mechatronics, 1P2-L14, 2020.

[8] M. Macklin, K. Storey, M. Lu, P. Terdiman, N. Chentanez, S. Jeschke, and M. Muller, "Small steps in physics simulation", 18th Annual ACM SIGGRAPH/Eurographics Symp. Computer Animation, pp. 1-7, 2019.

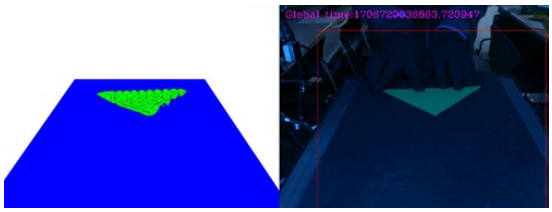

(a) First valley fold

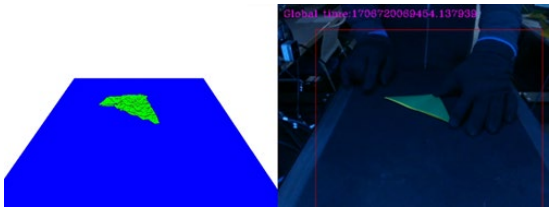

(b) Second valley fold

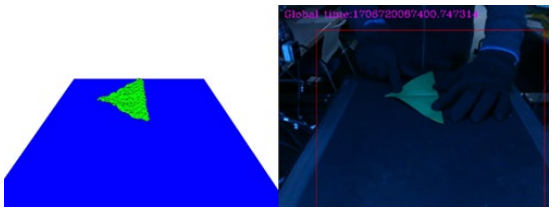

(c) Opening first valley fold

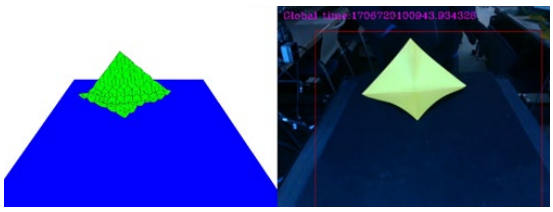

(d) Opening second valley fold

Fig. 6: Shape Estimation Using Origami Simulator